Formation of Multi-Phase Complex Coacervates and Partitioning of Biomolecules Within Them

Gregory A. Mountain and Christine D. Keating*

Department of Chemistry, The Pennsylvania State University, University Park, Pennsylvania 16802, USA

*keating@chem.psu.edu

Abstract:

Biological systems employ liquid-liquid phase separation to localize macromolecules and processes. The properties of intracellular condensates that allow for multiple, distinct liquid compartments, and the impact of their coexistence on phase composition and solute partitioning are not well understood. Here, we generate two and three coexisting macromolecule-rich liquid compartments by complex coacervation based on ion pairing in mixtures that contain two or three polyanions together with one, two, or three polycations. While in some systems polyelectrolyte order-of-addition was important to achieve coexisting liquid phases, for others it was not, suggesting that the observed multiphase droplet morphologies are energetically favorable. Polyelectrolytes were distributed across all coacervate phases, depending on the relative interactions between them, which in turn impacted partitioning of oligonucleotide and oligopeptide solutes. These results show the ease of generating multiphase coacervates and the ability to tune their partitioning properties via the polyelectrolyte sharing inherent to multiphase complex coacervate systems.

Introduction:

Eukaryotic cells contain numerous different membraneless organelles thought to be important in cellular processes ranging from stress response to transcription.[1-2] These structures, also known as intracellular condensates, are rich in macromolecules such as proteins and nucleic acids, and are now understood to form through liquid-liquid phase separation (LLPS).[3-5] The cell maintains many distinct intracellular condensates simultaneously, often in direct contact without mixing.[6-13] For example, the nucleoli of *Xenopus laevis* oocytes contain subcompartmentalized liquid phases composed of at least three coexisting subcompartments termed the fibrillar center, dense fibrillar component, and granular component.[6] It is thought that these adjacent compartments could be important for sequential RNA processing steps.[6, 14] While it is currently unclear to what extent active processes are important for maintaining distinct compositions of different condensate types in living cells, stable multiphase systems can be produced in vitro.[6, 9, 15-16] For example, purified recombinant proteins nucleophosmin (NPM1/B23), and fibrillarin (FIB1) when mixed with ribosomal RNA have been shown to generate structures that resemble the granular and dense fibrillar components of nucleoli.[6]

The simultaneous presence of multiple interaction types (such as charge-charge, cation-pi, hydrophobic, and sequence specific binding) between the biomolecules associated with biological phase separation, and the molecular complexity of the intracellular milieu complicate a straightforward interpretation of in vivo phase separation in terms of individual interaction types between particular molecules. Experiments using simpler phase-separating components as model systems can help improve understanding of minimal interaction types and conditions necessary to generate and maintain coexisting intracellular condensates. For example, complex coacervate systems have been employed previously to model the behavior of non-membrane bound cellular compartments.[17-22] Complex coacervation results from ion pairing between charge moieties of oppositely charged polyelectrolytes, and the counterion release associated with complexation.[23-25] This process can generate droplets of a polyelectrolyte-rich coacervate phase surrounded by a dilute continuous phase. While undoubtedly simpler than the sum of

interactions leading to phase separation in vivo, complex coacervation captures aspects such as the importance of stretches of charged residues and the destabilizing effect of added salt on phase separation. Biological macromolecules such as nucleic acids or polypeptides rich in charged residues readily undergo complex coacervation.[9, 22, 26-30]

Aqueous multiphase separated systems are common for non-associative polymer systems such as PEG, dextran, and Ficoll and have been used for separations.[16, 31] Elastin-like peptides (ELPs) with slightly differing repeat sequences have also been demonstrated to undergo LLPS to generate multi-compartment systems based on small differences in sequence composition and hydrophobicity.[15, 32] It is not immediately obvious that multiple distinct phases could be generated and maintained in the same solution environment based on ion pairing alone. Instead, one might anticipate a single complex coacervate phase that contained the majority of all polycations and polyanions present, surrounded by a single dilute phase. Alternatively, if differences in polyelectrolyte characteristics like length or charge density between the possible polyelectrolyte pairs were significant, one might expect to see multiple phases in which the more and less favorable interaction pairs ended up forming distinct phases at equilibrium. Boeynaems et al recently reported multiphase droplets in solutions of poly (proline-arginine) repeat peptide and mixtures of RNA homopolymers arising from differences in the magnitudes of cation-pi interactions between arginine residues and the different RNA bases.[9] Additional routes to multiphase coexistence could arise due to metastable nonequilibrium systems. For any system where additional coacervate phases are present, it is interesting to ask what impact coacervate coexistence will have on the distribution of biomolecular solutes such as oligonucleotides and peptides. Both biological and synthetic coacervates are known to recruit and sequester various solutes from their surroundings.[26-27, 33-34] This property is critical to their role as intracellular compartments.[1-2] Despite the simultaneous presence of many different membraneless organelles in vivo, the effect of multiple coexisting coacervate phases on solute recruitment and distribution has only begun to be explored.

Here, we demonstrate production of multiphase complex coacervate systems from several different sets of oppositely-charged polyelectrolytes, and show that while in some cases polyelectrolyte order-of-addition is crucial to achieve coexisting liquid phases, others are not sensitive to changes in the order-of-addition, suggesting that the observed droplet morphologies are energetically favorable at equilibrium. We find that formation of multiphase complex coacervates is relatively straightforward if each potential pair of polyelectrolytes is able to form a liquid phase under the shared solution conditions to be used in their combination. Fluorescently-labeled biomolecular solutes (RNA oligonucleotides and an oligopeptide) were added to the complex coacervate samples to observe their accumulation into coacervates that were prepared either together (as two-phase coacervates) or in separate containers (as single-phase coacervates). We observed differences in the distribution of these biomolecular probe molecules between the two scenarios that could be rationalized by considering the likely redistribution of polyelectrolytes between the coexisting coacervates. Our results show that multiphase complex coacervates can be readily formed and maintained with different local biomolecular occupancy, and that partitioning behavior of the coacervate phases is impacted by their coexistence. These effects can be understood in terms of polyelectrolytes being shared to various degrees between the coacervates based on their ability to compete for ion pairing interactions.

Materials and Methods:

Materials. Poly(uridylic acid potassium salt) (MW 600-1000 kDa), poly(acrylic acid) (MW 1.8 kDa), poly(allylamine hydrochloride) (MW 17.5 kDa), HEPES, HEPES sodium salt, magnesium sulfate, sodium chloride, (1-ethyl-3-(3-dimethylaminopropyl)carbodiimide hydrochloride) (EDC), ethylene diamine, 2-mercaptoethanol and Amicon Ultra centrifugal filters were purchased from Sigma-Aldrich (St. Louis, MO). Poly(L-lysine hydrochloride) (MW 16 kDa, n=100), poly(L-lysine hydrochloride) (MW 3.3 kDa, N=20), poly(L-glutamic acid sodium salt) (MW 15 kDa, n=100), and poly(L-aspartic acid sodium salt) (MW 14 kDa, n=100) were purchased from Alamanda Polymers (Huntsville, AL). Protamine sulfate

was purchased from MP Biomedicals (Santa Ana, CA). Anhydrous toluene was obtained from MilliporeSigma (Burlington, MA). Peptides were custom synthesized by Genscript (Piscataway, NJ) as hydrochloride salts with the amino acid sequence RRASLRRASL. The RRASLRRASL peptide was also obtained with a 5-carboxytetramethylrhodamine (TAMRA) N-terminus label. The oligonucleotides poly(adenylic acid) (A15), and poly(uridylic acid) (U15) were 5'-labeled with Alexa Fluor 546 (NHS ester) through an amino-modifier C6 linkage on the 5' phosphate and were obtained from Integrated DNA Technologies (Coralville, IA). Secure-Seal, one well spacers (9 mm diameter, 0.12 mm deep) from life technologies (Carlsbad, CA) or silicone spacers (9 mm diameter, 2mm deep) from Electron Microscopy Sciences (Hatfield, PA) were used for imaging. Micro cover glass (no. 1.5) 24 x 30 mm^2 were purchased from VWR (West Chester, PA). N-(triethoxysilylpropyl)-O-polyethylene oxide urethane purchased from Gelest (Morrisville, PA). Alexa Fluor 488 NHS, Alexa Fluor 555 NHS, Alexa Fluor 647 NHS, Alexa Fluor 488 hydrazide, Alexa Fluor 647 hydrazide, N-hydroxysulfosuccinimide (Sulfo-NHS), sulfosuccinimidyl acetate (NHS-Sulfo-acetate) and Zebra Spin Desalting Columns were purchased from Thermo Fisher Scientific, Co. (Waltham, MA). All chemicals were used without further purification.

Instrumentation. Confocal images were taken using a Leica TCS SP5 laser scanning confocal inverted microscope (LSCM) with Leica LAS AF software and an HCX PL APO CS 63.0x/1.40 oil UV objective. Fluorescence intensity data was acquired from raw fluorescence images using ImageJ.

Coacervate Preparation. Polyelectrolyte stock solutions were prepared in nuclease free water and either stored at 4°C for immediate use of -5°C for storage. Coacervate systems are prepared in a pairwise manner unless otherwise noted, where one pair of oppositely charged polyelectrolytes are introduced into buffered salt solution and allowed a 3min equilibration period prior to the direct addition of the polycation and polyanion of the second respective coacervate. For samples in which all polyelectrolytes were added simultaneously, all polyelectrolytes of like charge were premixed, after which the polycation mixture is added to the sample followed by addition of the polyanion mixture. Immediately after generation coacervates are analyzed or transferred to a microscope slide. In cases where fluorescent polyelectrolytes

are employed, only a small amount of the polyelectrolyte added to the system is fluorescently labeled and fluorescent polyelectrolyte is pre-mixed with non-labeled polyelectrolyte prior to addition to the sample. The exact amount of labeled polymer used varies in order to optimize fluorescence signal while minimizing the amount of labeled polymer used. The amount labeled polyelectrolyte used typically ranges between 0.1%-0.001% by weight of the unlabeled polymer, based on signal intensity.

Coacervate Imaging. Immediately after coacervate samples were fully prepared a small aliquot was transferred and sandwiched between two no1.5 coverslips with a secure seal 0.12mm x 9mm adhesive spacer (VWR). The slide is then allowed to sit for a minimum of 30min to allow droplets to equilibrate and fall to the bottom coverslip for imaging. Aliquoted and prepared sample slides were kept and reimaged after multiple days (where noted) in order to observe changes to the coacervate systems. The bottom slide is silanized by base treatment with KOH in isopropanol for 30min, dried overnight, then treated with 3mg/mL N-(triethoxysilylpropyl)-O-polyethylene oxide urethane dissolved in toluene for 4hours, and dried before use; otherwise coacervate droplets adopted non-spherical geometries during adsorption to the glass coverslips. All partitioning data represented in this work is collected as raw fluorescence intensity and converted to concentration using standard curves of the fluorescently labeled probe at known concentrations in identical buffer to coacervate samples (50 mM HEPES at pH 7.4, 25 mM NaCl, 2 mM $MgCl_2$). Probe concentration is presented as an average value with an associated standard deviation value that are calculated using 10 random coacervate droplets across triplicate samples for each formulation.

Fluorescent labeling of polyelectrolytes. Fluorescent variants of polyelectrolytes were synthesized for this work using commercially available dyes via conjugation chemistry to available functional groups. PAH (AlexaFluor488-NHS ester), Lys100 (AlexaFluor555-NHS ester), protamine (Fluorescein-NHS or Rhodamine-NHS) were labeled via primary amine labeling following manufacturer instructions. Fluorescently labeled Asp100 was prepared in-house by conjugating Alexa Fluor 488 hydrazide to carboxylic acid residues using an EDC linker. The labeling reaction was performed step-wise to ensure

maximum labeling efficiency and purity. 12.3 mg of Asp100 (14 kDa) was dissolved in 1 mL 0.1 PBS buffer. 25-molar equivalent sulfo-NHS-acetate was added to 100 µL of the Asp100 solution to cap the terminal amines. The solution was gently mixed at room temperature for 1 hour. Excess sulfo-NHS-acetate was removed using a Zebra Spin Desalting Column (7 kDa MWCO) that had been equilibrated with 0.1 M MES buffer, pH ~6. 0.1 molar equivalent EDC and 0.25 molar equivalent sulfo-NHS acetate were added to the purified polymer to form the reactive intermediate. After 15 minutes, the excess EDC was quenched using 10 molar excess 2-mercaptoethanol. The polymer was purified again with a desalting spin column equilibrated with 0.1 PBS buffer. The purified polymer was added directly to ~1 mg of Alexa 488 hydrazide and mixed at room temperature for 2 hours. Excess label was removed with a desalting spin column, and the solution was concentrated using an Amicon Ultra centrifugal filter (MWCO 3 kDa). The labeled polymer was then stored at -22°C. The same method was used to prepare fluorescently labeled Glu100, with modified procedure to account for differences in molecular weight of polymer.

Results and Discussion:

Table 1 displays the size, charge density, and multivalency information for the polymers used in this work, which include synthetic, bio-inspired, and biological polyelectrolytes. Complex coacervate systems will be referred to using the abbreviations in Table 1, in the following format: (polycation/polyanion). Each cation/polyanion combination was screened for phase separation and new phases classified as liquid or solid under constant buffer conditions of 50 mM HEPES pH 7.4, 25 mM NaCl, and 2 mM $MgCl_2$ at 25°C (Table S1). Polyelectrolytes were used at the concentrations specified in Table S1 (1-6 mM charge concentration, depending on the polymer) unless otherwise noted. We refer to polyelectrolytes throughout this work in terms of charge concentration (polymer concentration multiplied by the number of charges per molecule) as it allows us to compare polyelectrolytes of different length, charge density, etc. Two of our polycations contain arginine residues as the charged moieties; these can

be expected to interact with polyU via not only ion pairing but also cation-pi interactions.[9, 35] Since coacervation can depend on a range of conditions such as ionic strength, pH, and temperature, it is

Table 1. Polyelectrolytes Used to Prepare Complex Coacervates

Polyelectrolyte	*Abbrev.*	*Molecular Weight (g/mol)*	*Charge/Molecule*	*Mass Per Charge (g/mol)*
RRASLRRASL	2xRRASL	1,185	(+) 4	296
Protamine sulfate[b]	Prot	4,236[a]	(+) 21	202
Poly(L-lysine)	Lys20	3,300 [a]	(+) 20	160
	Lys100	16,000[a]	(+) 100	160
Poly(allylamine hydrochloride)	PAH	17,500[a]	(+) 300	58
Poly(acrylic acid)	PAA	1,800[a]	(-) 25	72
Poly(L-glutamic acid)	Glu100	15,000[a]	(-) 100	150
Poly(L-aspartic acid)[c]	Asp100	14,000[a]	(-) 100	140
Poly(uridylic acid)	polyU	600k - 1,000k[a]	(-) 1850 - 3085	324

[a]Average molecular weight
[b]Protamine is a mixture of naturally occurring arginine rich peptides. See Table S2 for sequence and composition information
[c]Poly(L-aspartic acid) synthesis results in random α-β isomerization of the polymer (See SI Discussion)

important to identify common conditions under which phase separation is possible for each of the intended polyelectrolyte pairs prior to designing a system capable of supporting co-existing coacervates. Here, the relatively low ionic strength was chosen to facilitate coacervation across the set of polyelectrolytes in Table 1. The short peptide, RRASLRRASL (single letter amino acid sequence), in particular requires low ionic strength for coacervation with polyU. Ionic strength tolerances can be shifted into the physiological range by increasing multivalency; addition of a third RRASL to this sequence increases its salt stability above 300 mM NaCl.[27]

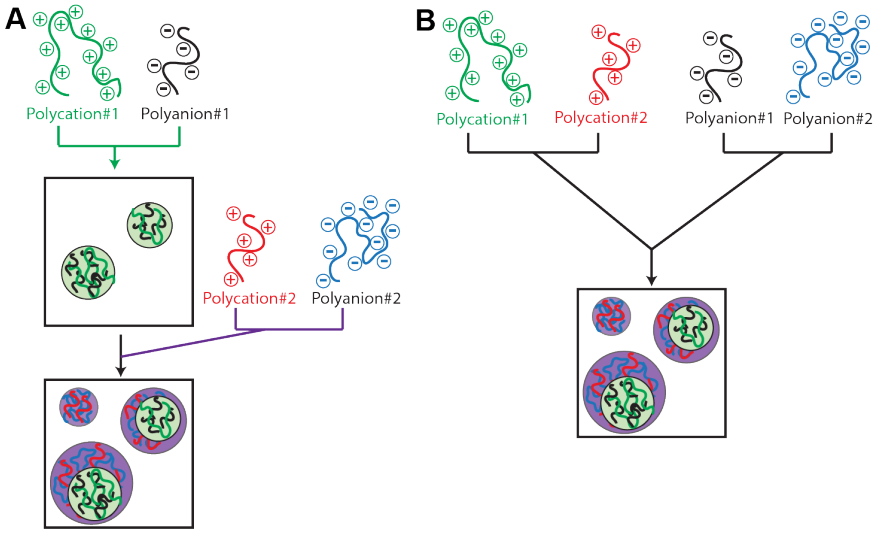

Scheme 1. **(A)** Sequential formation of multiphase coacervates. The first coacervate is formed by mixing one polyanion and one polycation, prior to addition of the second polyelectrolyte pair. **(B)** Like charge polymers are premixed and added to the sample simultaneously.

Two-phase coacervate droplets from four polyelectrolytes. We began by selecting two different four-polyelectrolyte combinations, each containing two polycations and two polyanions that, under our buffer conditions, would form coacervates in multiple pairwise polycation/polyanion combinations (Table 1). Set 1 contained PAH, Prot, PAA, and Glu100; here, either polycation is able to undergo coacervation with either anion. Set 2 contained 2xRRASL, Prot, polyU, and Glu100; here 2xRRASL can only form coacervates with polyU but Prot can form coacervates with either polyanion. Anticipating that for either set, the order of polyelectrolyte addition could be important in controlling which of the possible polycation/polyanion combinations predominated, we prepared coacervates in two ways: (1) first forming one polycation/polyanion pair (e.g., PAH/PAA), followed by the addition of the second polycation, and the second polyanion (e.g., Prot/Glu100) as shown in Scheme 1A, and (2) addition of all four polyelectrolytes simultaneously by premixing like-charged polymers before addition as shown in Scheme

1B. Samples were imaged with confocal fluorescence microscopy to visualize the distribution of fluorescently-tagged polyelectrolytes. For both Sets of polyelectrolytes and for both sequential or all-at-once mixing, we observed multiphase droplets that clearly contain two separate subcompartments, each enriched with a different complement of fluorescently-tagged polyelectrolytes (Figure S1, Figure 1). Both samples from Set 1 and Set 2 persist in morphology and fluorescence distribution for at least 6 days (Figure 1B,D). Protamine was labeled with either Rhodamine or fluorescein depending on open fluorescence channels, however, the identity of the label had no apparent impact on the observed fluorescence ordering (Figure S2). Line scans of the fluorescence intensity across coexisting phases are shown in Figure S3 Samples generated using the sequential order of addition method (Scheme1A, Figure S1, Table S3) have similar distribution of polymers across phases compared to simultaneous addition (Scheme1B, Figure 1, Table S4) based on the relative fluorescence intensity of each polyelectrolyte in either coacervate phase. It is likely that the polyU and PAA, which are not included in the line-scans because these molecules were not fluorescently labeled, are also present to some degree in both phases of these multiphase coacervate systems.

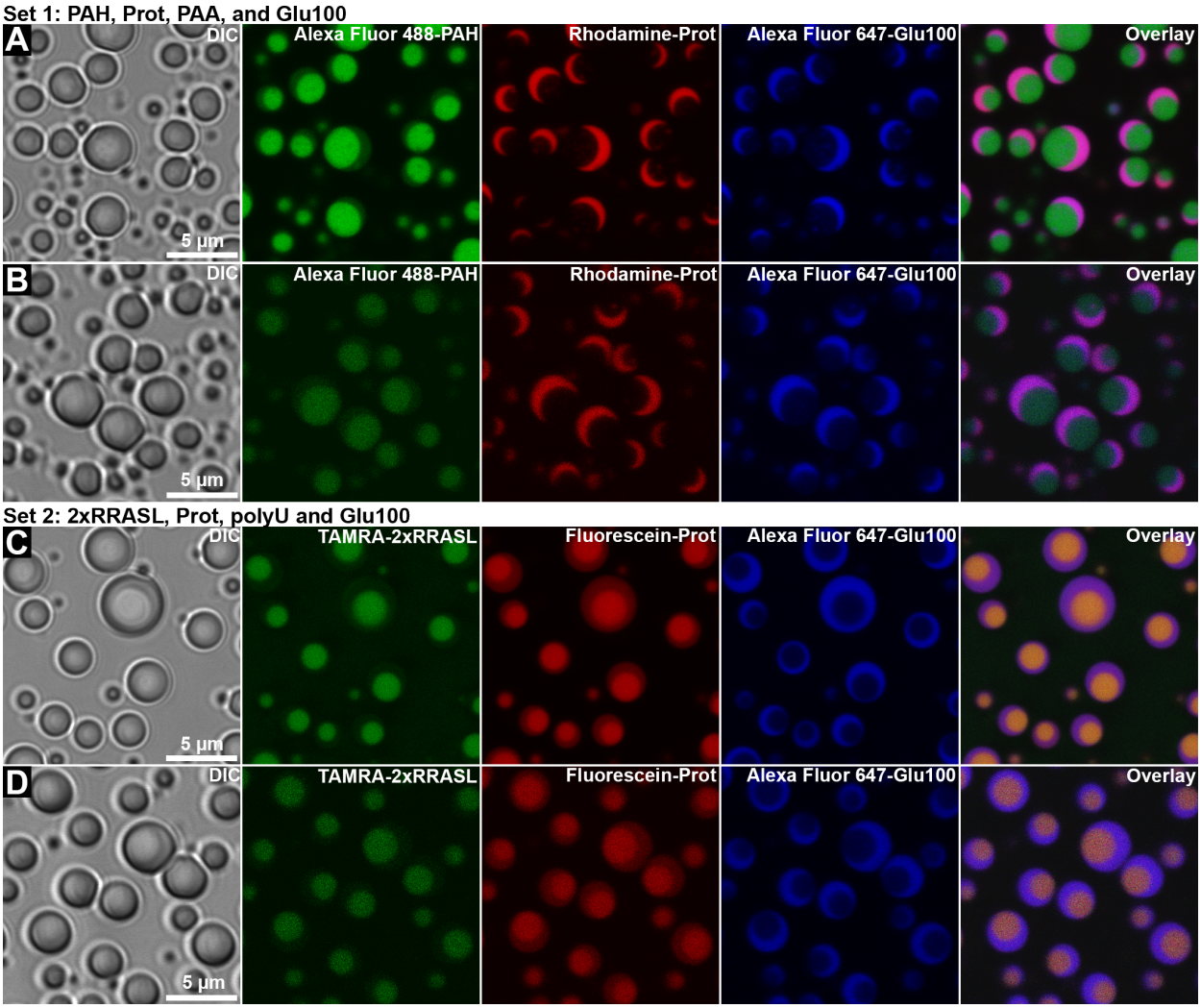

Figure 1: Fluorescence confocal microscopy images of double coacervate systems. Individual fluorescence channels and an overlay were false-colored and brightness adjusted to indicate which labeled molecule was present. All polyelectrolytes were added simultaneously. **(A)** Set 1 polyelectrolytes PAH, Prot, PAA, Glu100 with Alexa Fluor 488 labeled PAH (green), rhodamine labeled protamine (red), and Alexa Fluor 647 Glu100 (Blue). **(B)** The same PAH, Prot, PAA, Glu100 system, reimaged after 6 days. **(C)** Set 2 polyelectrolytes 2xRRASL, Prot, polyU, Glu100 system with 5-carboxytetramethylrhodamine (TAMRA) labeled 2xRRASL (green), fluorescein labeled protamine (red), and Alexa Fluor 647 Glu100 (Blue). **(D)** The same 2xRRASL, Prot, polyU, Glu100 system, reimaged after 6 days.

Rather than binary pairings of oppositely charged polyelectrolytes we observe one or multiple polyelectrolytes being shared between coacervate phases while maintaining distinct compositions. The coacervate phases formed in Set 1 samples are enriched in different polycations (one PAH-rich and one Prot-rich coacervate phase). The labeled polyanion, Glu100, is found primarily in the outer coacervate phase. The other polyanion in Set 1, PAA, is unlabeled and thus we cannot comment on its distribution across the coacervate phases but presume it to be primarily in the most Glu100-poor coacervate phase. Hence it appears that the major components of the two coexisting coacervates in Set1 are PAH/PAA (green) in the inner coacervate phase, and Prot/Glu100 (red/blue) in the outer surrounding phase in Figure 1A. Comparing the physical properties of polymers like charge density, and multivalency within a set we can gain some insight into polyelectrolyte distributions in these multiphase coacervates. Of the polycations in Set 1 (Figure 1A, B) PAH has a higher total charge per molecule (300 charges/molecule), and also a higher charge density (58 g/charge) compared to protamine with 21 charges/molecule and 202 g/charge respectively (Table 1). Of the Set 1 polyanions, PAA has 4x fewer total charges per molecule than Glu100 but an approximately 2x higher charge density. We can thus interpret the apparent main phase compositions of PAH/PAA (green) + Prot/Glu100 (red/blue) as resulting from coacervation between the two oppositely charged polyelectrolytes having the strongest interactions (PAH with PAA) to form one phase, and between the remaining polyelectrolytes that could not compete effectively for interactions with the "better" polyelectrolytes to form the other phase. Morphologies of multiphase droplet systems can be interpreted in terms of the relative interfacial tensions at the various interfaces.[6, 36-37] Here, the Glu100-rich phase has the greatest interfacial area with the dilute continuous phase, indicating that this interfacial tension ($\gamma_{out\text{-}Glu100}$) is lowest. This is consistent with the morphology, in which the PAH/PAA-rich phase is formed in the center, surrounded by the Prot/Glu100-rich phase.

Set 2 samples exhibit somewhat different behavior, having one phase highly enriched in both polycations (2xRRASL and Prot) surrounded by a second phase that also contains appreciable Prot signal. The apparent greater local concentration of both polycations in the same phase is somewhat

counterintuitive since the phase separation here is driven by ion pairing interactions between the polycations and polyanions; both types of species are required for complex coacervation. The lower total polycation-associated fluorescence signal from the Set 2 outer coacervate phase can be rationalized as a lower overall polymer concentration (i.e. higher water content) as compared to the interior phase. The labeled polyanion, Glu100, is found primarily in the outer coacervate phase. The other polyanion in Set 2, polyU, was unlabeled and thus we can only infer that polyU is primarily in the inner coacervate phase due to the high localization of both polycations, and comparatively low Glu100 signal in the inner phase. The major components of the two coexisting coacervates in Set 2 appear to be 2xRRASL/Prot/polyU (green/red) + Prot/Glu100 (red/blue) in Figure 1C. In Set 2 (Figure 1C,D), protamine contains more charges per molecule (21) and higher charge density as measured by mass per charge (202 g/mol) than the other polycation (2xRRASL, with 4 charges per molecule and 296 g/mol respectively) though 2xRRASL is present in a nearly 3x excess of molar charge compared to polyU (Table S1) we still see protamine most concentrated within the presumed polyU-rich phase. PolyU has a lower charge density (324 g/mol) than Glu100 (150 g/mol), but is approximately 25x more multivalent than Glu100 with 2500 and 100 charges per molecule respectively. In Set 2, the Glu100-rich phase also has the greatest interfacial area with the dilute continuous phase, indicating that this interfacial tension ($\gamma_{out\text{-}Glu100}$) is lowest and is consistent with the hypothesis that this outer Glu-rich phase has lower overall polymer content (greater water content) than the inner phase, helping to explain the higher concentration of both polycations in the inner phase of Figure 1C. The overall observed wetting morphologies for Set 2 in Figure 1 are consistent with $\gamma_{out–Glu100} < \gamma_{Glu100–PAH} \leq \gamma_{out–PAH}$ and $\gamma_{out–Glu100} < \gamma_{Glu100–2xRRASL} < \gamma_{out-–2xRRASL}$, where "out" indicated the continuous phases, and coacervate phases are labeled based on their predominant fluorescently-labeled components. We hypothesize that the relative interaction strengths could explain differences in the degree to which polyelectrolytes appear in multiple coacervate phases, with the polycations capable of stronger interactions being distributed across both coacervate phases due to their ability to more effectively

compete for interactions with oppositely-charged polyelectrolytes than those having less charge density and/or less multivalency.

These experiments demonstrate the relative ease with which coexisting coacervate phases can be produced, whether controlling the order of polyelectrolyte addition, or simply mixing two polycations and two polyanions together at once. The coexisting coacervates formed two-phase droplets in which one phase wet the other and differences in polyelectrolyte composition persisted indefinitely (at least 6 days). Our data also shows, however, that in all cases (different addition methods, analysis after 30 min or 6 d), the composition of the individual coacervate phases have been altered by polyelectrolyte sharing between coacervate phases.

Double coacervates from three polyelectrolytes. We hypothesized that by identifying multiple polyanions that would undergo complex coacervation with the same polycation, it would be possible to generate coexisting coacervate systems using only three polyelectrolytes, where the polycation is shared across all coacervate phases (Scheme 2). To test this hypothesis we chose Lys100, which is capable of coacervation with either Asp100 or polyU (Table S1). Using these polymers in charge concentration of 6.4 mM Lys100, 5 mM Asp100, and 1.4 mM polyU such that the charge concentration of Lys100 is equal to the sum of the charge concentrations of both polyanions, we find that coexisting droplet systems can indeed be generated which share the same polycation (Figure 2). Line-scans of the Alexa Fluor 555-Lys100 in the system (Figure S4) show Lys100 in both coacervate phase though predominantly concentrated in the non-Asp100 phase (presumed polyU phase). It is also interesting to note that similar to our findings in Figure 1, the order of addition in this system has no bearing on the final morphology of this system and the two polyanions (polyU and Asp100) can be mixed or added stepwise before or after the addition of pLys100 with no observable change in the resulting coexisting coacervate system. A mixture of Lys20, Lys100, and polyU generates only one coacervate phase (Figure S5) even though Lys20/polyU, or Lys100/polyU are possible on an individual basis (Table S1). This suggests that the relatively small difference in length between Lys20 and Lys100 is not sufficient to drive distinct liquid

phases in this system, and that differences in polyelectrolyte characteristics such as charge density, multivalency, and chemical identity of functional groups may be necessary in order to generate coexisting coacervates.

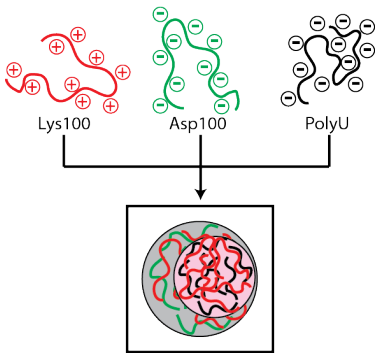

Scheme 2. Combining a single polycation (Lys100) with a mixture of polyanions (Asp100, and polyU) at appropriate charge concentration results in multiphase coacervates that share the polycation.

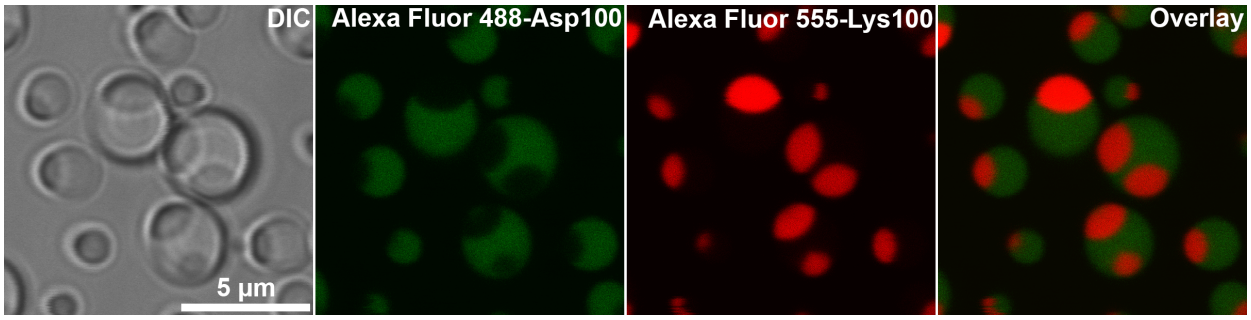

Figure 2: Fluorescence confocal microscopy images of double coacervate system of pLys100, pAsp, and polyU. Individual channels false-colored to indicate which labeled molecule was present and an overlay of fluorescence channels are displayed. Both polyanions (Asp100, polyU) were added simultaneously, followed by the polycation (Lys100).

Partitioning in single- versus multi-coacervate systems:

One of the most important properties of membraneless organelles and coacervate droplets is their ability to compartmentalize solutes, which depends upon their chemical composition and physical properties .[26-27, 33, 38] In the results described above, we observed varying degrees of polyelectrolyte sharing between coexisting coacervate phases that appears to be determined by the relative properties of the polyelectrolytes involved. This can be expected to alter the properties of the phases. In single-

coacervate systems, researchers have previously observed that adding additional polyelectrolytes can impact the physical and chemical properties of the phase. For example, Priftis et al reported that varying the relative amounts of poly(allylamine or poly(ethylenimine) with poly(acrylic acid) and poly(N,N-dimethylaminoethyl methacrylate) in the system directly affects the physical and chemical properties of the resulting coacervate.[39] These effects are relevant to the biological function of intracellular condensates. For example, adding RNA to liquid droplets of the intrinsically disordered Whi3 protein alters physical properties of the phase, such as viscosity and intradroplet diffusion, and facilitates phase separation at lower concentrations of Whi3.[40] We were therefore interested to learn what effect the presence of multiple coexisting coacervate phases had upon solute partitioning. The results from Figure 1, Figure S3, and Table S4 already suggested that partial exchange of polyelectrolytes between the coacervates was occurring; this could be expected to alter solute partitioning. We quantified the distribution of several probes in both single-coacervate and dual-coacervate systems. Probes used were Alexa Fluor 546-poly(uridylic acid) n=15, Alexa Fluor 546-poly(adenylic acid) n=15, and 5-carboxytetramethylrhodamine (TAMRA)-Kemptide (single letter amino acid sequence: LRRASLG), which will be referred to as U15, A15, and kemptide respectively. The two RNA oligos were chosen in order to observe the effect of Watson-Crick base pairing on partitioning into polyU-containing systems. Small oligonucleotide (oligo) and peptide probes were chosen as they are among the types of macromolecules affected by sequestration in biology and also to allow us to view the differences in partitioning observed between negatively charge and positively charged solutes.

Partitioning results for all three labeled solutes across five different coacervate phases in several combinations are shown in Table 2. Solute concentrations in each coacervate phase were determined by confocal fluorescence emission, based on calibration curves, and are compared to the amount of solute added and total sample volume. All fluorescent solutes are added to a final concentration of 0.1 μM. Due to the low fluorescence intensities in the continuous dilute phase, it was not possible to accurately determine solute concentration outside the coacervates from the imaging data to derive a partitioning

coefficient, K = (solute concentration in coacervate)/(solute concentration in continuous phase). We can however estimate a lower limit for (K) by comparing the coacervate phase concentration of solute to our limit of detection, which is the same as the final overall concentration of added solute (0.1 μM). Therefore the difference in the added probe concentration and the measured coacervate phase concentration (measured coacervate phase concentration times 10) serves as an estimated lower limit for K.

Table 2: Partitioning Data for Multi-coacervate Systems

		Probe: *Alexa Fluor 546-U15*	*Alexa Fluor 546-A15*	*TAMRA-Kemptide*
Coacervate Phase Measured: [b]	*Coexisting Phase Present:* [c]	*Coacervate Phase Conc. (μM)* [a]	*Coacervate Phase Conc. (μM)* [a]	*Coacervate Phase Conc. (μM)* [a]
PAH/PAA[b]	none	16 ± 3	10 ± 5	≤ 0.1
	+ 2xRRASL/polyU	6 ± 1	7 ± 2[d]	1.7 ± 0.3
	+ Prot/Glu100	6 ± 1	5 ± 2	0.4 ± 0.2
2xRRASL/polyU[b]	none	5.0 ± 0.5	30 ± 8	39 ± 1
	+ PAH/PAA	13 ± 1	14 ± 6[d]	18 ± 1
	+ Prot/Glu100	49 ± 8	104 ± 33[d]	10.8 ± 0.1
Prot/Glu100[b]	none	39 ± 5	45 ± 12	1.7 ± 0.2
	+ 2xRRASL/polyU	23 ± 3	40 ± 21[d]	2.0 ± 0.2
	+ PAH/PAA	37 ± 3	34 ± 14	1.2 ± 0.1
Lys100/polyU[b]	none	42 ± 5	74 ± 2	3.2 ± 0.8
	+ Lys100/Asp100	3.8 ± 0.2	56 ± 2	≤ 0.1
Lys100/Asp100[b]	none	0.9 ± 0.1	≤ 0.1	≤ 0.1
	+ Lys100/polyU	2.7 ± 0.1	6 ± 1	≤ 0.1

[a]All partitioning probes were added to a final concentration of 0.1μM.
[b]Denotes the phase for which local solute concentration was measured, whether or not a coexisting phase was present (if present, coexisting phase identity is noted in the column to the right)
[c]Additional phases that were present when local solute concentration was measured in the phase noted in the column to the left. "None" indicates that no coexisting phase was present."
[d]Presence of granular, solid-like component

Single-coacervate systems. For the 2xRRASL/polyU system in Table 2, we see that while U15 partitions to the coacervate phase with a concentration of 5 ± 0.5 μM (50-fold greater than added), partitioning of A15 to the coacervate phase is even stronger at a concentration of 30 ± 8 μM (300-fold greater than added and corresponding to a minimum K of 300). We attribute this increase in partitioning to the presence of Watson-Crick base pairing between A15 and the polyU component of the coacervate phase. Likewise, in

the Lys100/polyU system there is a two-fold greater enrichment of A15 within the coacervate phase at 74 ± 2 μM compared to U15 at 42 ± 5 μM. In all other tested coacervate systems the difference in partitioning for U15 vs A15 were insignificant, consistent with the absence of base pairing interactions. In polyU containing coacervate systems we observe RNA oligo partitioning is roughly 8x higher for U15, and 2.5x higher for A15 when Lys100 is used as the polycation over 2xRRASL. Lys100 contains approximately 25x more positive charges per molecule than 2xRRASL, while U15 and A15 are negatively charged and thus experience more favorable interactions with the longer polycation within the coacervate phase.

We observe that partitioning for kemptide is stronger for the polyU containing systems employing 2xRRASL as the polycation over Lys100 by approximately 12-fold. This observation is particularly interesting because the 2xRRASL/polyU coacervate system is generated with a nearly three-fold excess of 2xRRASL (in terms of charge concentration) with respect to polyU to obtain maximum phase separation. However, kemptide partitioning is likely lower when the more multivalent Lys100 polycation is used due to increased difficulty in competing for ion pairing sites on polyU. Kemptide is of similar multivalency to the 2xRRASL polycation making competition for electrostatic sites on polyU easier, resulting in increased observed partitioning. The partitioning behavior can be understood in terms of 3 factors: (1) the magnitude of ion pairing interactions between the probe and the oppositely charged polyelectrolyte of the coacervate, which drives accumulation, (2) the ion pairing capability of the coacervate's like-charged polyelectrolyte, which opposes accumulation, and (3) the availability of specific binding interactions such as Watson-Crick base pairing, which can greatly increase solute partitioning into coacervates.[26]

Multi-coacervate systems. To evaluate whether phase coexistence impacts probe partitioning, we prepared samples with two coexisting coacervates using the sequential method of Scheme 1A, under the same conditions from the previous single-coacervate partitioning experiments. The concentration of each polyelectrolyte is the same in dual-coacervate samples as in the corresponding single-coacervate samples.

This means that the total polyelectrolyte concentration in the sample is higher in dual coacervate experiments than single-coacervate systems, and the total volume of coacervate phase is expected to be larger (possibly 2x; due to the small sample volumes we were unable to quantify coacervate volumes). As a baseline, one might therefore expect that a ~2x concentrated sample of the same type of coacervate would result in a ~2x lower concentration of labeled solute inside the coacervate phase. Our findings, when comparing solute concentrations in coacervates formed alone versus in dual-coacervate systems showed a more nuanced behavior, with different trends seen for different combinations of coacervates and for different solutes. The distribution of labeled A15 RNA in two different double coacervate systems is shown in Figure 3. In the Set 1 polyelectrolyte system from above (PAH, Prot, PAA, Glu100), A15 is accumulated by both phases, but at a ~7x higher level in the Prot/Glu100 phase as compared to the PAH/PAA phase (Figure 3A). For the Set 2 system (2xRRASL, Prot, polyU, Glu100), A15 concentration is highest in the 2xRRASL/Prot/polyU phase Figure 3B, which can be understood on the basis of its attraction to polyU via Watson-Crick base pairing. Phase assignments here are based on polycation distribution in Figure 1.

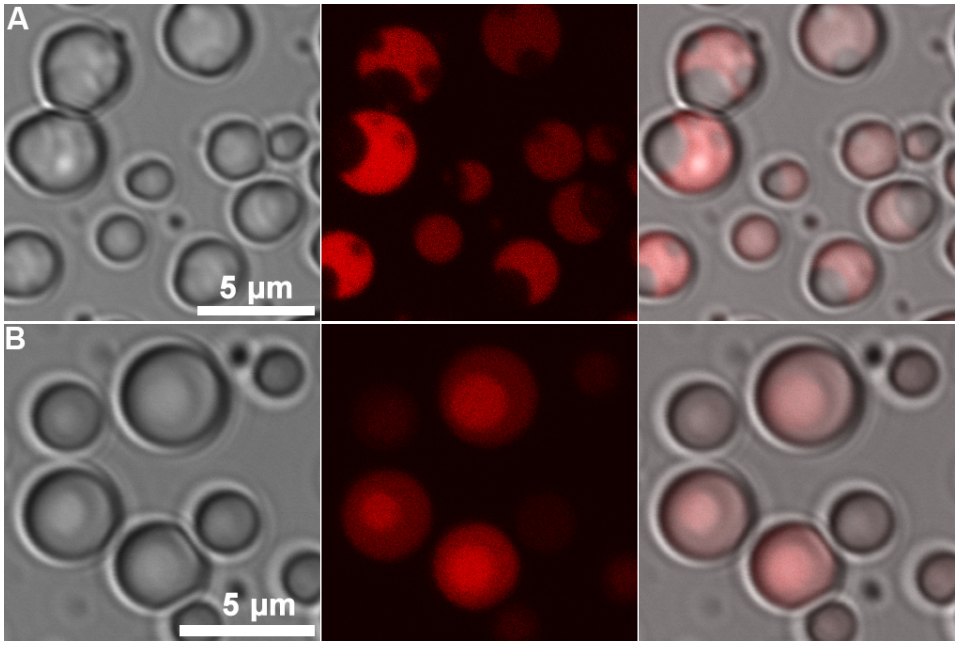

Figure 3. Distribution of Alexa Fluor 546 fluorescently-labeled A15 RNA oligonucleotide (red) in multiphase coacervate systems **(A)** Set 1 (PAH, Prot, PAA Glu100) double coacervate system, and **(B)** Set 2 (2xRRASL, Prot, polyU, Glu100). Concentration values for fluorescent A15 in each phase can be found in Table 2.

Overall, we observed that probe partitioning into coacervate phases was generally enhanced, over the single-phase scenarios, when the second coacervate phase included a stronger polyelectrolyte (oppositely charged of the probe). Exceptions were seen in scenarios where solid/gel structures occur, as in the case of A15 partitioning into 2xRRASL/polyU + PAH/PAA. In this case, the solid-like structures are likely due to PAH + polyU interactions, as these two polyelectrolytes form solids rather than liquids when mixed directly (Table S1, Figure S6). While gel/solid structures are also relevant as intracellular condensates,[10, 41] we sought to avoid them here to facilitate the partitioning measurements.

Polymers that are shared between phases can act as modifiers, effectively altering the physiochemical properties of the coacervate phase and affecting the partitioning of probe molecules. For instance, in the Set 2 polyelectrolytes, we found substantial levels of protamine present in the "2xRRASL/polyU" phase. Protamine is a stronger polycation than 2xRRASL and thus experiences more favorable electrostatic interaction with our oligonucleotide probes (U15, and A15) effectively modifying the 2xRRASL/polyU phase to increase partitioning for the oligo probes. Following the same logic, kemptide which carries the same charge as protamine experiences decreased partitioning likely due to greater difficulty in competing for ion pairing with polyU against protamine. The observed partitioning for oligos in the Prot/Glu100 phase in the aforementioned coexisting system decreases by almost 2x versus the singular Prot/Glu100 coacervate likely due to an increased amount of oligo in the other coacervate phase and loss of protamine to the 2xRRASL/polyU phase.

The partitioning behavior of coexisting coacervate systems show that the characteristics of a coacervate phase are a collective of all of the molecules present in that phase. Often, key protein component(s) of an intracellular condensate are studied by themselves in vitro (e.g., after overexpression and purification). These established methods are useful in identifying the minimal biological components

necessary for phase separation; however, our results show that the properties of these simpler in vitro condensates may be quite different from their in vivo counterparts, which exist in a complex milieu that contains numerous other macromolecules with varying propensities to join the droplet phase. These observations add to other related work indicating that the presence of additional molecules such as RNAs or macromolecular crowders can have an impact on coacervate properties.[40, 42-44] Thus, while much can be learned by studying proteins, polypeptides and polymers in vitro in isolated environments, it is important to consider these contributing factors when studying LLPS in biological systems.

Triple Coacervate Systems: Living cells contain many more than two coexisting intracellular liquid condensates. In order to explore the possibility of generating more than two coexisting coacervate phases we chose to employ all six polyelectrolytes from Figure 1. Anticipating solid complexation issues between PAH and polyU (see Figure S6) we devised a sequential order of addition strategy to generate three coexisting coacervate phases. All three polycations (2xRRASL, PAH, and protamine) were combined in solution and the order of addition of polyanions was then used to control the order of phase generation. Upon addition of PAA we observe onset of turbidity which we interpret as the formation of a predominantly PAH/PAA phase and allow a 3 min equilibration period. We then add Glu100 to generate a predominantly Prot/Glu100 phase, postulating that addition of polyU before Glu100 might potentially lead to Prot/polyU interaction, since coacervation of these two polyelectrolytes is also possible under these buffer conditions (Table S1). PolyU was added last which we expected to in principle generate a predominantly 2xRRASL/polyU phase in the triple coacervate system. The resulting multiphase coacervates can be seen in Figure 4 with two different populations of fluorescently labeled polymers showing distribution of polyelectrolytes within multicoacervate systems composed of at least three coexisting coacervates phases. Figure 4A displays the coexisting system with one polymer from each of the three intended polyelectrolyte pairs (PAH, 2xRRASL, and Glu100) fluorescently labeled. Figure 4B contains two fluorescently labeled polymers from a single intended polyelectrolyte pair (prot and Glu100) along with labeled 2xRRASL. We later discovered that the order of addition for Glu100 and polyU had

no significant bearing on the morphology of the resulting triple coacervate system (Figure S7). The only requirement was that PAA/PAH be generated first, due to aggregation issues from solid complexation of PAH and polyU.

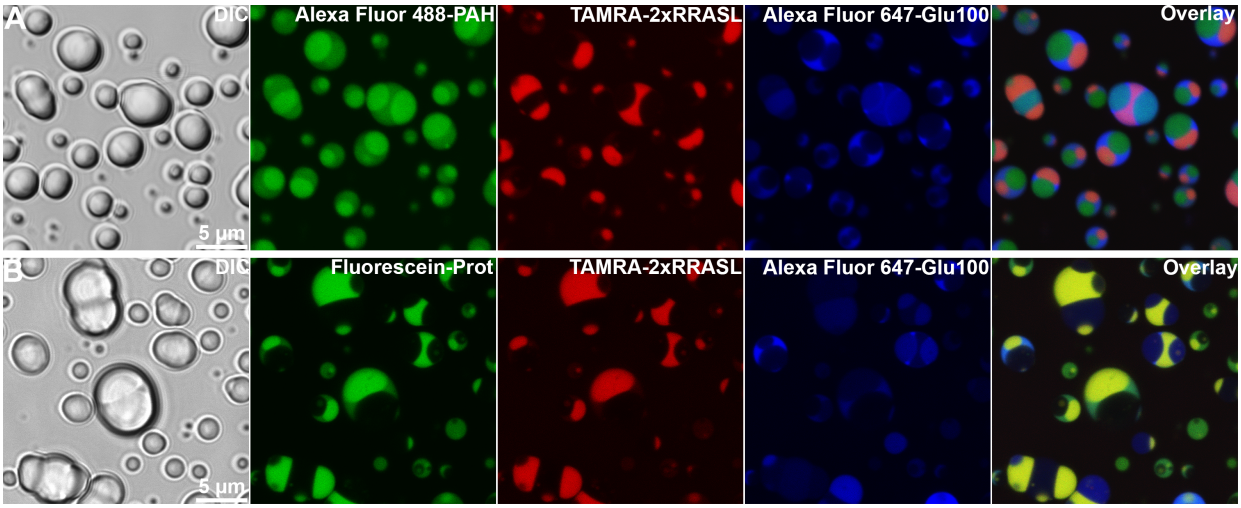

Figure 4. Fluorescence confocal microscopy images of coexisting coacervates consisting of three polyelectrolyte rich phases. Both image sets include PAH, Prot, 2xRRASL, PAA, Glu100, and polyU polyelectrolytes but different polymers are fluorescently labeled in either case. **(A)** Sample with fluorescent PAH, 2xRRASL, and Glu100 labels. **(B)** sample with fluorescent Prot, 2xRRASL, and Glu100 labels. Brightness of all channels was adjusted for visual clarity.

Three distinct coacervate phases are clearly visible in Figure 4, with two smaller phases, one of which is enriched in all three of the polycations, while the other is enriched in only the PAH polycation. These two coacervate phases can form chained structures (predominantly red and green phases in Figure 4A and can be observed wetting each other, but are predominantly observed being wet by a third outer coacervate phase that contains the lowest amount of PAH of the three phases, but is still moderately enriched in PAH, 2xRRASL, and protamine and is highly enriched in the one fluorescently-labeled polyanion present in the experiment (Glu100); this polyanion is also present in the other two coacervate phases. The other two polyanions present, PAA and polyU, are unlabeled and hence their distribution cannot be

determined from these images. We presume that they are also distributed across multiple phases. Because in addition to ion pairing, polycation-pi interactions are also possible between arginine residues and RNA nucleobases, we consider it likely that the polyU is the predominant anionic component of the phase rich in Prot and 2xRRASL. In Figure 4A we see PAH distributed across all three coacervate phases but in Figure 4B we see that there is a single coacervate phase deficient in the other two polycations (2xRRASL, and protamine), suggesting in conjunction with fluorescence distributions from double coacervate systems of PAH/PAA + prot/Glu100 in Figure 1A where the predominantly PAH coacervate phase is deficient in protamine and Glu100 that that the 2xRRASL, protamine deficient phase in Figure 4B may consist mostly of PAH and PAA. The observed morphology indicates the relative magnitudes of the interfacial tensions between the four phases present (three coacervate phases and the fourth, continuous phase). We can infer that the interfacial tension between the exterior continuous phase and the coacervate most enriched in Glu100 (blue) is lower than that of the outside continuous phase and either of the other coacervate phases ($\gamma_{out-blue} < \gamma_{out-green}, \gamma_{out-red}$), and that the interfacial tensions of the red or green phase from Figure 4A with the predominantly blue (Glu100) coacervate is lower than the interfacial tension between the red and green phases from Figure 4A ($\gamma_{green-blue}, \gamma_{red-blue} < \gamma_{green-red}$).

Conclusion:

Multiphase complex coacervate droplets were generated from several different sets of polyelectrolytes. These included cases where two (or three) polycations and two (or three) polyanions were mixed as well as cases where a single polyelectrolyte polycation was mixed with two polyanions to form two complex coacervate phases. Indeed, the ease of forming multiphase coacervates suggests that this scenario may be more of a rule than an exception, even for systems based predominantly on ion-pairing interactions rather than specific biorecognition. We found that order-of-addition was important only for systems in which particularly strong ion-pairing interactions were possible between the polyelectrolytes (e.g., PAH + polyU). Knowledge of the phase behavior of all possible polycation–

polyanion combinations under the same solution conditions, particularly ionic strength, provided important guidance for which sets of polyelectrolytes would be compatible for forming all-liquid multiphase coacervates and when solids could be expected.

The strength of partitioning of a probe molecule to specific coacervate phases is controlled by specific and non-specific interactions between the probe molecule and the individual polyelectrolytes of the coacervate phases. Therefore, with the ability to produce and maintain multiple, distinct coacervate phases, it should be possible to preferentially sequester different solutes to different and/or the same phase. It is possible that additional control over the contact area and wetting behavior between coexisting phases may be asserted by altering individual phase compositions through addition of solutes or adjusting polymer content of the coacervate. Certain intracellular condensates such as the nucleolus are thought to already take advantage of multiphase morphologies to spatially separate biochemical processes; the multiphase complex coacervate systems presented here are a step towards design of artificial versions of these multiphase microreactors. Control over multiple membraneless compartments in synthetic systems such as the ones demonstrated here is of interest not only as a minimal experimental model for living cells, but also as a means of incorporating increasingly sophisticated compartmentalization and functionality in bottom-up constructed artificial cells.[45-51]

In our work, coexisting complex coacervate phases generally maintained a predominant polycation and polyanion, but polyelectrolytes were also shared between phases to varying degrees depending on the system. This polyelectrolyte sharing altered the phase composition and physicochemical properties of coexisting coacervates. These changes impacted accumulation of solutes such as oligonucleotides and oligopeptides. The solute partitioning findings presented here highlight the complexity of molecular distribution in multiphase systems, and point to a new mechanism for tuning local solute concentrations by taking advantage of how polyelectrolyte sharing impacts partitioning. At the same time, they underscore the likelihood of significant differences in solute partitioning for simple in

vitro experiments that contain only a subset of the native macromolecular components of intracellular condensates in vivo.

Supporting information

The Supporting Information is available free of charge on the ACS Publications website at ( )

Tables containing polymer compatibility screening data, sequence data for protamine, and stability data for polymer distributions for sequential and simultaneous addition; discussion on isomerization of poly(L-aspartic acid), and considerations for fluorescently labeling polyelectrolytes; fluorescence images for multiphase coacervates made by sequential addition of polyelectrolytes, comparison of fluorescent label used for protamine, single phase formation with Lys20/Lys100/polyU, aggregation of PAH containing multicompartment systems, and comparisons of order of addition for triple coacervate systems; and Line scan comparisons of fluorescence distribution for double coacervates made with polymer pairs vs a shared polyelectrolyte

Acknowledgements:

The authors thank Jacob M. Schaffer for helpful discussion and assistance in early experiments related to this work. We also thank Andrew Rowland for sharing with us Alexa Fluor labeled Glu100 and Asp100 polyelectrolytes for imaging. This work was supported by the National Science Foundation, grant MCB-1715984.

References

1. Sawyer, I. A.; Bartek, J.; Dundr, M., Phase separated microenvironments inside the cell nucleus are linked to disease and regulate epigenetic state, transcription and RNA processing. *Semin. Cell Dev. Biol.* **2019,** *90*, 94-103.
2. Forman-Kay, J. D.; Kriwacki, R. W.; Seydoux, G., Phase Separation in Biology and Disease. *J. Mol. Biol.* **2018,** *430* (23), 4603-4606.
3. Brangwynne, C. P.; Eckmann, C. R.; Courson, D. S.; Rybarska, A.; Hoege, C.; Gharakhani, J.; Julicher, F.; Hyman, A. A., Germline P Granules Are Liquid Droplets That Localize by Controlled Dissolution/Condensation. *Science* **2009,** *324* (5935), 1729-1732.
4. Brangwynne, C. P.; Mitchison, T. J.; Hyman, A. A., Active liquid-like behavior of nucleoli determines their size and shape in Xenopus laevis oocytes. *Proc. Natl. Acad. Sci. U. S. A.* **2011,** *108* (11), 4334-4339.
5. Wheeler, R. J.; Hyman, A. A., Controlling compartmentalization by non-membrane-bound organelles. *Philos. Trans. R. Soc., B* **2018,** *373* (1747), 20170193.
6. Feric, M.; Vaidya, N.; Harmon, Tyler S.; Mitrea, Diana M.; Zhu, L.; Richardson, Tiffany M.; Kriwacki, Richard W.; Pappu, Rohit V.; Brangwynne, Clifford P., Coexisting Liquid Phases Underlie Nucleolar Subcompartments. *Cell* **2016,** (165), 1686-1697.
7. Fei, J.; Jadaliha, M.; Harmon, T. S.; Li, I. T. S.; Hua, B.; Hao, Q.; Holehouse, A. S.; Reyer, M.; Sun, Q.; Freier, S. M.; Pappu, R. V.; Prasanth, K. V.; Ha, T., Quantitative analysis of multilayer organization of proteins and RNA in nuclear speckles at super resolution. *J. Cell Sci.* **2017,** *130* (24), 4180.
8. Wheeler, J. R.; Matheny, T.; Jain, S.; Abrisch, R.; Parker, R., Distinct stages in stress granule assembly and disassembly. *eLife* **2016,** *5*, e18413.
9. Boeynaems, S.; Holehouse, A. S.; Weinhardt, V.; Kovacs, D.; Van Lindt, J.; Larabell, C.; Van Den Bosch, L.; Das, R.; Tompa, P. S.; Pappu, R. V.; Gitler, A. D., Spontaneous driving forces give rise to protein−RNA condensates with coexisting phases and complex material properties. *Proc. Natl. Acad. Sci. U. S. A.* **2019,** *116* (16), 7889.
10. Putnam, A.; Cassani, M.; Smith, J.; Seydoux, G., A gel phase promotes condensation of liquid P granules in Caenorhabditis elegans embryos. *Nat. Struct. Mol. Biol.* **2019,** *26* (3), 220-226.
11. Berry, J.; Brangwynne, C. P.; Haataja, M., Physical principles of intracellular organization via active and passive phase transitions. *Rep. Prog. Phys.* **2018,** *81* (4), 046601.
12. Alberti, S., The wisdom of crowds: regulating cell function through condensed states of living matter. *J. Cell Sci.* **2017,** *130* (17), 2789.
13. Banani, S. F.; Lee, H. O.; Hyman, A. A.; Rosen, M. K., Biomolecular condensates: organizers of cellular biochemistry. *Nat. Rev. Mol. Cell Biol.* **2017,** *18*, 285.
14. Tatomer, D. C.; Terzo, E.; Curry, K. P.; Salzler, H.; Sabath, I.; Zapotoczny, G.; McKay, D. J.; Dominski, Z.; Marzluff, W. F.; Duronio, R. J., Concentrating pre-mRNA processing factors in the histone locus body facilitates efficient histone mRNA biogenesis. *J. Cell Biol.* **2016,** *213* (5), 557.
15. Simon, J. R.; Carroll, N. J.; Rubinstein, M.; Chilkoti, A.; Lopez, G. P., Programming molecular self-assembly of intrinsically disordered proteins containing sequences of low complexity. *Nat. Chem.* **2017,** *9* (6), 509-515.
16. Mace, C. R.; Akbulut, O.; Kumar, A. A.; Shapiro, N. D.; Derda, R.; Patton, M. R.; Whitesides, G. M., Aqueous Multiphase Systems of Polymers and Surfactants Provide Self-Assembling Step-Gradients in Density. *J. Am. Chem. Soc.* **2012,** *134* (22), 9094-9097.
17. Koga, S.; Williams, D. S.; Perriman, A. W.; Mann, S., Peptide–nucleotide microdroplets as a step towards a membrane-free protocell model. *Nat. Chem.* **2011,** *3* (9), 720-724.
18. Nakashima, K. K.; Baaij, J. F.; Spruijt, E., Reversible generation of coacervate droplets in an enzymatic network. *Soft Matter* **2018,** *14* (3), 361-367.
19. Perry, S. L., Phase separation: Bridging polymer physics and biology. *Curr. Opin. Colloid Interface Sci.* **2019,** *39*, 86-97.

20. Nakashima, K. K.; Vibhute, M. A.; Spruijt, E., Biomolecular Chemistry in Liquid Phase Separated Compartments. *Front. Mol. Biosci.* **2019,** *6*, 21.
21. Aumiller, W. M.; Keating, C. D., Experimental models for dynamic compartmentalization of biomolecules in liquid organelles: Reversible formation and partitioning in aqueous biphasic systems. *Adv. Colloid Interface Sci.* **2017,** *239*, 75-87.
22. Ukmar-Godec, T.; Hutten, S.; Grieshop, M. P.; Rezaei-Ghaleh, N.; Cima-Omori, M.-S.; Biernat, J.; Mandelkow, E.; Söding, J.; Dormann, D.; Zweckstetter, M., Lysine/RNA-interactions drive and regulate biomolecular condensation. *Nat. Commun.* **2019,** *10* (1), 2909.
23. Kruyt, H. R., *Colloid Science Vol. II*. Elsevier: Amsterdam: 1949.
24. Wang, Q.; Schlenoff, J. B., The Polyelectrolyte Complex/Coacervate Continuum. *Macromolecules* **2014,** *47* (9), 3108-3116.
25. Gucht, J. v. d.; Spruijt, E.; Lemmers, M.; Cohen Stuart, M. A., Polyelectrolyte complexes: Bulk phases and colloidal systems. *J. Colloid Interface Sci.* **2011,** *361* (2), 407-422.
26. Aumiller, W. M.; Cakmak, F. P.; Davis, B. W.; Keating, C. D., RNA-Based Coacervates as a Model for Membraneless Organelles: Formation, Properties, and Interfacial Liposome Assembly. *Langmuir* **2016,** *32* (39), 10042-10053.
27. Aumiller, W. M.; Keating, C. D., Phosphorylation-mediated RNA/peptide complex coacervation as a model for intracellular liquid organelles. *Nat. Chem.* **2016,** *8* (2), 129-137.
28. Li, L.; Srivastava, S.; Andreev, M.; Marciel, A. B.; de Pablo, J. J.; Tirrell, M. V., Phase Behavior and Salt Partitioning in Polyelectrolyte Complex Coacervates. *Macromolecules* **2018,** *51* (8), 2988-2995.
29. Pak, Chi W.; Kosno, M.; Holehouse, Alex S.; Padrick, Shae B.; Mittal, A.; Ali, R.; Yunus, Ali A.; Liu, David R.; Pappu, Rohit V.; Rosen, Michael K., Sequence Determinants of Intracellular Phase Separation by Complex Coacervation of a Disordered Protein. *Mol. Cell* **2016,** *63* (1), 72-85.
30. Banerjee, P. R.; Milin, A. N.; Moosa, M. M.; Onuchic, P. L.; Deniz, A. A., Reentrant Phase Transition Drives Dynamic Substructure Formation in Ribonucleoprotein Droplets. *Angew. Chem. Int. Ed.* **2017,** *56* (38), 11354-11359.
31. Zaslavsky, B. Y., *Aqueous Two-Phase Partitioning: physical chemistry and bioanalytical applications*. Marcel Dekker, Inc.: New York, 1995.
32. Quiroz, F. G.; Chilkoti, A., Sequence heuristics to encode phase behaviour in intrinsically disordered protein polymers. *Nat. Matter.* **2015,** *14* (11), 1164-1171.
33. Black, K. A.; Priftis, D.; Perry, S. L.; Yip, J.; Byun, W. Y.; Tirrell, M., Protein Encapsulation via Polypeptide Complex Coacervation. *ACS Macro Lett.* **2014,** *3* (10), 1088-1091.
34. McCall, P. M.; Srivastava, S.; Perry, S. L.; Kovar, D. R.; Gardel, M. L.; Tirrell, M. V., Partitioning and Enhanced Self-Assembly of Actin in Polypeptide Coacervates. *Biophys. J.* **2018,** *114* (7), 1636-1645.
35. Brangwynne, Clifford P.; Tompa, P.; Pappu, Rohit V., Polymer physics of intracellular phase transitions. *Nat. Phys.* **2015,** *11*, 899.
36. Guzowski, J.; Korczyk, P. M.; Jakiela, S.; Garstecki, P., The structure and stability of multiple micro-droplets. *Soft Matter* **2012,** *8* (27), 7269-7278.
37. Torza, S.; Mason, S. G., Coalescence of Two Immiscible Liquid Drops. *Science* **1969,** *163* (3869), 813-814.
38. Frankel, E. A.; Bevilacqua, P. C.; Keating, C. D., Polyamine/Nucleotide Coacervates Provide Strong Compartmentalization of Mg2+, Nucleotides, and RNA. *Langmuir* **2016,** *32* (8), 2041-2049.
39. Priftis, D.; Xia, X. X.; Margossian, K. O.; Perry, S. L.; Leon, L.; Qin, J.; de Pablo, J. J.; Tirrell, M., Ternary, Tunable Polyelectrolyte Complex Fluids Driven by Complex Coacervation. *Macromolecules* **2014,** *47* (9), 3076-3085.
40. Zhang, H.; Elbaum-Garfinkle, S.; Langdon, E. M.; Taylor, N.; Occhipinti, P.; Bridges, Andrew A.; Brangwynne, Clifford P.; Gladfelter, Amy S., RNA Controls PolyQ Protein Phase Transitions. *Mol. Cell* **2015,** *60* (2), 220-230.
41. Shin, Y.; Brangwynne, C. P., Liquid phase condensation in cell physiology and disease. *Science* **2017,** *357* (6357), eaaf4382.

42. Marianelli, A. M.; Miller, B. M.; Keating, C. D., Impact of macromolecular crowding on RNA/spermine complex coacervation and oligonucleotide compartmentalization. *Soft Matter* **2018,** *14* (3), 368-378.
43. Lin, Y.; Protter, David S. W.; Rosen, Michael K.; Parker, R., Formation and Maturation of Phase-Separated Liquid Droplets by RNA-Binding Proteins. *Mol. Cell* **2015,** *60* (2), 208-219.
44. Guo, L.; Shorter, J., It's Raining Liquids: RNA Tunes Viscoelasticity and Dynamics of Membraneless Organelles. *Mol. Cell* **2015,** *60* (2), 189-192.
45. Crowe, C. D.; Keating, C. D., Liquid–liquid phase separation in artificial cells. *Interface Focus* **2018,** *8* (5), 20180032.
46. Martin, N., Dynamic Synthetic Cells Based on Liquid–Liquid Phase Separation. *ChemBioChem* **2019,** *0* (0).
47. Booth, R.; Qiao, Y.; Li, M.; Mann, S., Spatial Positioning and Chemical Coupling in Coacervate-in-Proteinosome Protocells. *Angew. Chem. Int. Ed.* **2019,** *58* (27), 9120-9124.
48. Deng, N.-N.; Huck, W. T. S., Microfluidic Formation of Monodisperse Coacervate Organelles in Liposomes. *Angew. Chem. Int. Ed.* **2017,** *56* (33), 9736-9740.
49. Deshpande, S.; Brandenburg, F.; Lau, A.; Last, M. G. F.; Spoelstra, W. K.; Reese, L.; Wunnava, S.; Dogterom, M.; Dekker, C., Spatiotemporal control of coacervate formation within liposomes. *Nat. Commun.* **2019,** *10* (1), 1800.
50. Mason, A. F.; Yewdall, N. A.; Welzen, P. L. W.; Shao, J.; van Stevendaal, M.; van Hest, J. C. M.; Williams, D. S.; Abdelmohsen, L. K. E. A., Mimicking Cellular Compartmentalization in a Hierarchical Protocell through Spontaneous Spatial Organization. *ACS Cent. Sci.* **2019,** *5* (8), 1360-1365.
51. Schwille, P.; Spatz, J.; Landfester, K.; Bodenschatz, E.; Herminghaus, S.; Sourjik, V.; Erb, T. J.; Bastiaens, P.; Lipowsky, R.; Hyman, A.; Dabrock, P.; Baret, J.-C.; Vidakovic-Koch, T.; Bieling, P.; Dimova, R.; Mutschler, H.; Robinson, T.; Tang, T. Y. D.; Wegner, S.; Sundmacher, K., MaxSynBio: Avenues Towards Creating Cells from the Bottom Up. *Angew. Chem. Int. Ed.* **2018,** *57* (41), 13382-13392.

For Table of Contents